Planar Lipid Bilayers (BLMs) and their Applications
H. T. Tien and A. Ottova-Leitmannova (Editors)

Chapter 4

Effect of anisotropic properties of membrane constituents on stable shapes of membrane bilayer structure

Ales Iglic[a] and Veronika Kralj-Iglic[b]

[a]Laboratory of Applied Physics, Faculty of Electrical Engineering, University of Ljubljana, Trzaska 25, SI-1000 Ljubljana, Slovenia

[b]Institute of Biophysics, Faculty of Medicine, University of Ljubljana, Lipiceva 2, SI-1000 Ljubljana, Slovenia

1. INTRODUCTION

From a physical point of view, we can outline two properties of the lipid bilayer. The first is that the dimension of the lipid bilayer in at least one of the lateral directions is much larger than its thickness, while the second is that the shape attained by the bilayer reflects the shape of the molecules that constitute the bilayer and the interactions between them. Due to the first property, the bilayer resembles a two dimensional surface, while the second property contributes to the particularities of the shape that this "surface" attains in three-dimensional space (Fig. 1).

A two-dimensional surface in three-dimensional space can be described in an elegant way by using the equations of differential geometry based on a local 2×2 curvature tensor. The equilibrium shape attained by the membrane corresponds to the minimum of the free energy of the system at relevant geometrical constraints. The link between the membrane shape and its free energy is provided by expressing the free energy of each part of the membrane by the invariants of the local curvature tensor.

The lipid bilayer is of scientific interest especially due to its relation to the membrane of cells and organelles [1]. Following many years of thorough study, the fluid mosaic model has been proposed [2] where it is assumed that the cell membrane, regardless of its specific function, can be described as a lipid bilayer with intercalated proteins or other large molecules. The lipid bilayer exhibits the properties of a two dimensional liquid that is laterally isotropic,

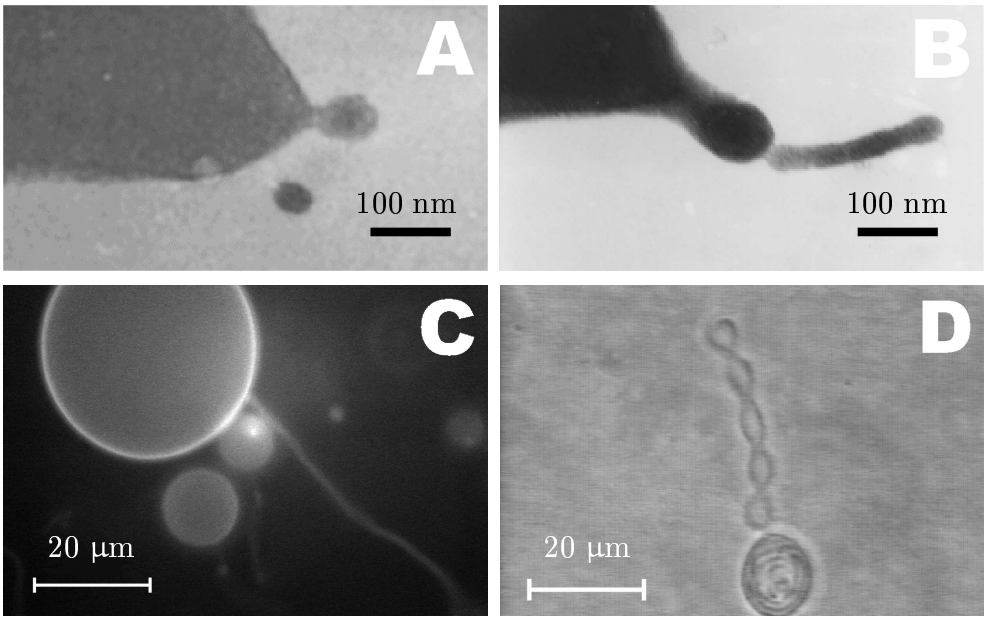

Figure 1. Examples of bilayer membrane shapes: A: transmission electron microscope (TEM) image of a spherical bud at the top of the echinocyte spicule induced by adding dodecylzwittergent to an erythrocyte suspension (from [10]), B: TEM image of a cylindrical bud at the top of the echinocyte spicule induced by adding the dimeric detergent dioctyldiQAS to an erythrocyte suspension (from [10]), C: fluorescence microscope image of the vesicle made of POPC and 1.5 % NBD-PC probe in sugar solution; the length of the myelin-like protrusion was several diameters of the spherical part (from [32]); D: phase contrast microscope image of a vesicle made of POPC in pure water; the shape exhibits an undulated protrusion while there is a multilamellar structure within the globular part (from [12]).

within which the proteins and other large molecules are more or less laterally mobile. In agreement with the fluid mosaic model [2], the membrane was considered as a laterally isotropic continuum so that its energy was expressed by the invariants of the local curvature tensor: the mean curvature and the Gaussian curvature [3].

The properties of the cell membrane can also be studied by introducing exogenously added molecules into the membrane. A convenient system for such study is represented by mammalian erythrocytes. These cells have no internal structure, so that the properties of their membrane (composed of a lipid bilayer with intercalated proteins and a membrane skeleton), are reflected in their shape. It was observed that intercalation of various substances induces observable shape changes in mammalian erythrocytes [4, 5, 6].

Study of the effects of detergents on the erythrocyte membrane showed that continuous intercalation of detergent molecules into the membrane leads

to microvesiculation of the membrane [7, 8, 9]. The released microexovesicles are so small that they cannot be observed by an optical microscope. However, the vesicles could be isolated and observed by an electron microscope [8]. It was found that the microexovesicles are spherical and cylindrical [8, 10] while the endovesicles are spherical, cylindrical and torocytic [11], depending on the species of exogenously added detergent. The difference between the main curvatures of the membrane in these structures is rather large. It can be expected that in the regions where there is a large difference between the main curvatures the membrane can no longer be described as a laterally isotropic continuum. A new physical description should be created taking into account the specific structure of the membrane constituents.

In this contribution, evidence is given that thin strongly anisotropic structures that are attached to the mother vesicle/cell can be found in one-component phospholipid bilayers and in erythrocytes under certain conditions. Starting from a microscopic description of the membrane constituents, we describe the thin anisotropic structures of the bilayer membrane by a mechanism that is based on the orientational ordering of the anisotropic membrane constituents. It is derived that the relevant invariants of the curvature tensor for description of such systems are the mean curvature and the curvature deviator [10, 12, 13]. The shapes of the membraneous structures are studied within the frame of these invariants and in correspondence with the experimentally observed shapes.

2. INTERDEPENDENCE BETWEEN THE CONFIGURATION OF THE INCLUSIONS AND THE SHAPE OF THE MEMBRANE

The membrane inclusion can be any membrane constituting molecule or any assembly of molecules that can be distinguished from the surrounding membrane constituents. The surrounding membrane constituents are then treated as a curvature field, the membrane inclusion being subject to this field. The inclusion may be located in a single monolayer or it may protrude through both layers.

We imagine that there exists a shape that would completely fit the inclusion. This shape is referred to as the shape intrinsic to the inclusion. The corresponding main curvatures are denoted by $C_{1\mathrm{m}}$ and $C_{2\mathrm{m}}$ [14, 15]. Fig. 2 gives a schematic presentation of four different intrinsic shapes. The inclusion is called isotropic if $C_{1\mathrm{m}} = C_{2\mathrm{m}}$ while it is called anisotropic if $C_{1\mathrm{m}} \neq C_{2\mathrm{m}}$.

It would be energetically most favourable if the membrane had the intrinsic shape over all its area. However, if we consider a closed shape subject to geometrical constraints, the membrane cannot have such a curvature at

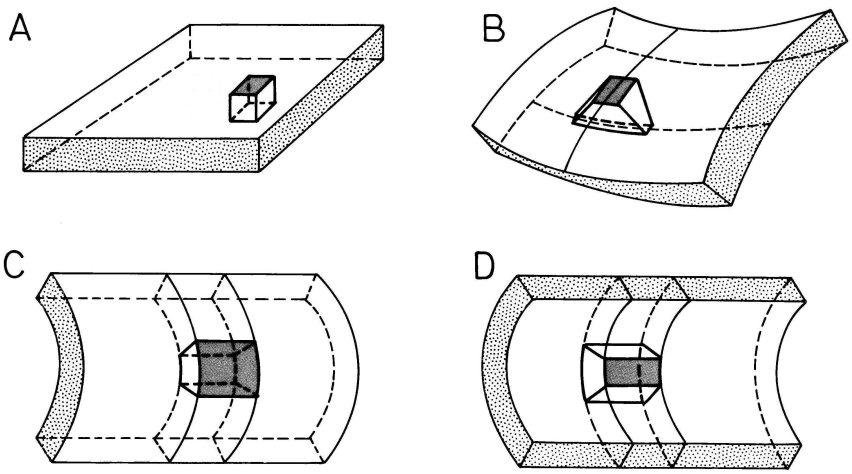

Figure 2. A schematic presentation of four different intrinsic shapes: A: flat shape ($C_{1\mathrm{m}} = C_{2\mathrm{m}} = 0$), B: saddle shape ($C_{1\mathrm{m}} > 0$, $C_{2\mathrm{m}} < 0$), C: cylinder ($C_{1\mathrm{m}} > 0$, $C_{2\mathrm{m}} = 0$), D: inverted cylinder ($C_{1\mathrm{m}} < 0$, $C_{2\mathrm{m}} = 0$). The shape A is isotropic while the shapes B,C and D are anisotropic (from [12]).

all its points. In general, the local membrane shape differs from the intrinsic shape. This means that the principal curvatures and the principal directions of the actual shape differ from the principal curvatures and the principal directions, respectively, of the intrinsic shape. The mutual orientation of the two principal systems describes the orientation of the inclusion if $C_{1\mathrm{m}} \neq C_{2\mathrm{m}}$ *i.e.* if the inclusion is anisotropic.

In a one-component bilayer membrane every membrane constituent can be treated as an inclusion that is confined to the corresponding monolayer. In a membrane containing proteins or some other molecules the inclusion is formed by the seed molecule and adjacent membrane constituent molecules that are significantly distorted due to its presence. The difference in the treatment of the respective systems lies in the statistical mechanical description that yields consistently related expressions for the membrane free energy and positional and orientational distribution functions. A lattice with an adjustable lattice constant is introduced. In the case when we consider every constituent as an inclusion embedded in the continuum formed by the other constituents, all of the lattice sites are occupied [12]. In the case when the number of inclusions is much smaller than the number of membrane constituents (*e.g.* when the inclusions are formed by the membrane proteins or induced by intercalated drugs), most of the lattice sites are empty [14, 15]. As the inclusions are laterally mobile over the membrane area, they would accumulate in the regions of favourable curvature, while they would be depleted from the regions of unfavourable curvature. In both statistical mechanical

approaches there would be a different degree of orientational ordering of the inclusions in different regions. Correspondingly, the whole membrane would attain a shape exhibiting large regions of favourable local shape and small regions of unfavourable shape, as such a configuration would yield the minimal free energy of the whole membrane.

The free energy of the membrane is subject to the local thermodynamic equilibrium (which is considered by using canonical ensemble statistics) and the global thermodynamic equilibrium with respect to the positional and orientational distribution functions of the inclusions and with respect to the membrane shape, *i.e.* the principal membrane curvatures at each point of the membrane. The relevant geometrical constraints such as the requirement for a fixed membrane area and enclosed volume are taken into account. In this work we present some approximate solutions of this variational problem that seem to be relevant for the particular experimentally observed features.

3. SINGLE-INCLUSION FREE ENERGY

The origin of the coordinate system is chosen at the site of the inclusion. The membrane shape at this site is described by the diagonalized curvature tensor $\underline{C}$,

$$\underline{C} = \begin{bmatrix} C_1 & 0 \\ 0 & C_2 \end{bmatrix}, \tag{1}$$

while the intrinsic shape is described by the diagonalized curvature tensor $\underline{C}_{\mathrm{m}}$

$$\underline{C}_{\mathrm{m}} = \begin{bmatrix} C_{1\mathrm{m}} & 0 \\ 0 & C_{2\mathrm{m}} \end{bmatrix}. \tag{2}$$

The principal directions of the tensor $\underline{C}$ are in general different from the principal directions of the tensor $\underline{C}_{\mathrm{m}}$, the systems being mutually rotated by an angle ω.

We introduce the mismatch tensor $\underline{M}$ [13, 16],

$$\underline{M} = \underline{R}\,\underline{C}_{\mathrm{m}}\,\underline{R}^{-1} - \underline{C} \tag{3}$$

where $\underline{R}$ is the rotation matrix,

$$\underline{R} = \begin{bmatrix} \cos\omega & -\sin\omega \\ \sin\omega & \cos\omega \end{bmatrix}. \tag{4}$$

The single-inclusion energy is defined as the energy that is spent in adjusting the inclusion into the membrane and is determined by terms composed of two invariants of the mismatch tensor $\underline{M}$. Terms up to the second order in

the tensor elements are taken into account. The trace and the determinant are considered as the fundamental invariants [13, 16],

$$E = \frac{K}{2}\left(\mathrm{Tr}(\underline{M})\right)^2 + \bar{K}\,\mathrm{Det}(\underline{M}), \tag{5}$$

where K and $\bar{K}$ are constants. Performing the necessary operations and using the expressions (1) - (5) yields the expression for the single-inclusion energy [14, 15]

$$E = \frac{\xi}{2}(H - H_\mathrm{m})^2 + \frac{\xi + \xi^\star}{4}(\hat{C}^2 - 2\hat{C}_\mathrm{m}\,\hat{C}\cos 2\,\omega + \hat{C}_\mathrm{m}^2), \tag{6}$$

where

$$H = \frac{1}{2}(C_1 + C_2), \quad H_\mathrm{m} = \frac{1}{2}(C_{1\mathrm{m}} + C_{2\mathrm{m}}) \tag{7}$$

are the respective mean curvatures while

$$\hat{C} = \frac{1}{2}(C_1 - C_2), \quad \hat{C}_\mathrm{m} = \frac{1}{2}(C_{1\mathrm{m}} - C_{2\mathrm{m}}). \tag{8}$$

The constants used in Eq. (6) are $\xi = 2\bar{K} + 4K$ and $\xi^\star = -6\bar{K} - 4K$.

The partition function of a single inclusion q is [17]

$$q = \frac{1}{\omega_0}\int_0^{2\pi} \exp\left(-\frac{E(\omega)}{k\,T}\right)\mathrm{d}\omega, \tag{9}$$

with ω_0 an arbitrary angle quantum and k the Boltzmann constant. In the partition function of the inclusion the contribution of the orientational states q_orient is distinguished from the contribution of the other states q_c, $q = q_\mathrm{c}\,q_\mathrm{orient}$ [15],

$$q_\mathrm{c} = \exp\left(-\frac{\xi}{2k\,T}(H - H_\mathrm{m})^2 - \frac{\xi + \xi^\star}{4k\,T}(\hat{C}^2 + \hat{C}_\mathrm{m}^2)\right), \tag{10}$$

$$q_\mathrm{orient} = \frac{1}{\omega_0}\int_0^{2\pi} \exp\left(\frac{(\xi + \xi^\star)\hat{C}_\mathrm{m}\,\hat{C}\cos(2\omega)}{2k\,T}\right)\mathrm{d}\omega. \tag{11}$$

Integration in Eq. (11) over ω yields

$$q_\mathrm{orient} = \frac{1}{\omega_0}\mathrm{I}_0\left(\frac{(\xi + \xi^\star)\hat{C}_\mathrm{m}\,\hat{C}}{2k\,T}\right), \tag{12}$$

where I_0 is the modified Bessel function. The free energy of the inclusion is then obtained by the expression $F_\mathrm{i} = -k\,T \ln q$,

$$F_\mathrm{i} = \frac{\xi}{2}(H - H_\mathrm{m})^2 + \frac{\xi + \xi^\star}{4}\,(\hat{C}^2 + \hat{C}_\mathrm{m}^2) - k\,T \ln\left(\mathrm{I}_0\Big(\frac{(\xi + \xi^\star)\hat{C}_\mathrm{m}\,\hat{C}}{2k\,T}\Big)\right). \quad (13)$$

We introduce the curvature deviator

$$D = |\hat{C}| \quad (14)$$

that is an invariant of the curvature tensor as it can be expressed by its trace and determinant,

$$D = \sqrt{(\mathrm{Tr}(\underline{C})/2)^2 - \mathrm{Det}(\underline{C})} = \sqrt{H^2 - C_1\,C_2}. \quad (15)$$

Here, it was considered that $\mathrm{Tr}(\underline{C}) = 2H$ and $\mathrm{Det}(\underline{C}) = C_1\,C_2$. Since the modified Bessel function and the quadratic function are even functions of the difference $\hat{C}$, the quantity $\hat{C}$ in (Eq. (13)) can be replaced by the curvature deviator D (Eq. (14)). Thereby the single inclusion free energy is expressed in a simple and transparent way by two independent invariants of the curvature tensor: the trace and the absolute value of the difference of the main curvatures *i.e.* by the mean curvature H and the curvature deviator D,

$$F_\mathrm{i} = \frac{\xi}{2}(H - H_\mathrm{m})^2 + \frac{\xi + \xi^\star}{4}\,(D^2 + D_\mathrm{m}^2) - k\,T \ln\left(\mathrm{I}_0\Big(\frac{(\xi + \xi^\star)\,D_\mathrm{m}\,D}{2k\,T}\Big)\right), \quad (16)$$

where $D_\mathrm{m} = |\,\hat{C}_\mathrm{m}\,|$.

The average orientation of the inclusion may be given by $\langle\cos(2\omega)\rangle$ [18],

$$\langle\cos(2\omega)\rangle = \frac{\mathrm{I}_1\left(\frac{(\xi+\xi^\star)D_\mathrm{m}\,D}{2k\,T}\right)}{\mathrm{I}_0\left(\frac{(\xi+\xi^\star)D_\mathrm{m}\,D}{2k\,T}\right)}. \quad (17)$$

where I_1 is the modified Bessel function.

Fig. 3 shows the average orientation of the inclusion as a function of the curvature deviator D. For small D, *i.e.* in nearly isotropic regions, the inclusions are randomly oriented. The orientational ordering increases with increasing D and approaches the state where all the inclusions are aligned at large D, *i.e.* in strongly anisotropic regions.

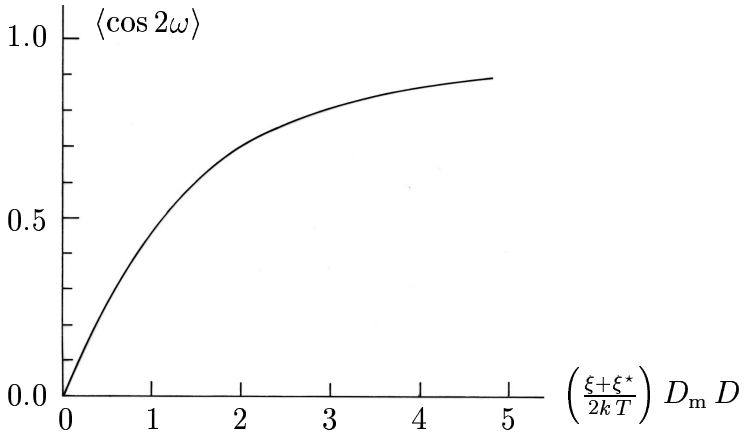

Figure 3. Average orientation of the inclusion $\langle\cos(2\omega)\rangle$ as a function of the curvature deviator D (from [18]).

4. SHAPES OF EXTREME AVERAGES OF CURVATURE TENSOR INVARIANTS

The shapes of the extreme average invariants of the curvature tensor are distinct shapes in the set of possible shapes. In order to obtain the shapes of the membrane of an extreme average mean curvature

$$\langle H\rangle = \frac{1}{A}\int H\,\mathrm{d}A \tag{18}$$

and of an extreme average curvature deviator

$$\langle D\rangle = \frac{1}{A}\int D\,\mathrm{d}A \tag{19}$$

at a given area of the membrane surface A and a given volume enclosed by the membrane V, the variational problems are stated by constructing the respective functionals [18, 16]

$$\mathcal{G}_H = \langle H\rangle - \lambda_A\cdot\Big(\int \mathrm{d}A - A\Big) + \lambda_V\cdot\Big(\int \mathrm{d}V - V\Big), \tag{20}$$

$$\mathcal{G}_D = \langle D\rangle + \lambda_A\cdot\Big(\int \mathrm{d}A - A\Big) - \lambda_V\cdot\Big(\int \mathrm{d}V - V\Big), \tag{21}$$

where λ_A and λ_V are the Lagrange multipliers. The analysis is restricted to axisymmetric shapes. The shape is given by the rotation of the function $y(x)$ around the x axis. In this case the principal curvatures are expressed by $y(x)$ and its derivatives with respect to x as $C_1 = \pm 1/y\sqrt{1+y'^2}$ and

$C_2 = \mp y''/\sqrt{1+y'^2}^3$, where ($y' = \partial y/\partial x$ and $y'' = \partial^2 y/\partial x^2$). The area element is $\mathrm{d}A = 2\pi\sqrt{1+y'^2}\, y\, \mathrm{d}x$, and the volume element is $\mathrm{d}V = \pm\pi\, y^2\, \mathrm{d}x$. By $\pm$ it is taken into account that the function $y(x)$ may be multiple valued. The sign may change at the points where $y' \to \infty$. The variations

$$\delta\mathcal{G}_H = \delta \int g_H(x,\, y,\, y',\, y'')\, \mathrm{d}x = 0 \tag{22}$$

and

$$\delta\mathcal{G}_D = \delta \int g_D(x,\, y,\, y',\, y'')\, \mathrm{d}x = 0 \tag{23}$$

are performed by solving the corresponding Poisson - Euler equations

$$\frac{\partial g_i}{\partial y} - \frac{\mathrm{d}}{\mathrm{d}x}\left(\frac{\partial g_i}{\partial y'}\right) + \frac{\mathrm{d}^2}{\mathrm{d}x^2}\left(\frac{\partial g_i}{\partial y''}\right) = 0, \quad i = H,\, D. \tag{24}$$

By inserting g_H and g_D into Eq. (24) we can express both variational problems by a Poisson-Euler equation of single form. After obtaining the necessary differentiations, this Poisson - Euler equation is [18, 16]

$$\delta_1 \frac{2y''}{\left(1+y'^2\right)^2} + \lambda_A\left(\frac{1}{\sqrt{1+y'^2}} - \frac{yy''}{(\sqrt{1+y'^2})^3}\right) - \delta_2 y\, \lambda_V = 0, \tag{25}$$

where δ_1 and δ_2 may be $+$ or $-$, depending on the actual situation. It follows from the above that the solutions for the extremes of the average invariants of the curvature tensor are equal. The nature of the obtained extreme may, however, be different. So it is possible that some solution corresponds to a maximal average mean curvature and maximal average curvature deviator. Some other solution may correspond to the minimum average mean curvature and maximum average curvature deviator *etc.*

Some simple analytic solutions of Eq. (25) were found: the cylinder $y = const$ [19, 10] and the circle of the radius r_cir, $y = y_0 \pm \sqrt{r_\mathrm{cir}^2 - (x-x_0)^2}$ where $(x_0,\, y_0)$ is the centre of the circle. If $x_0 \neq 0$ and $y_0 = 0$ the ansatz fulfills equation (25) for two different radii [19], representing spheres with two different radii. If $x_0 = 0$ and $y_0 \neq 0$, the circle is the solution of the equation (25) only when the Lagrange multipliers are interdependent; for $r_\mathrm{cir} < y_0$, the solution represents a torus and a torocyte [18].

As the sum of the solutions of the differential equation within each of the above categories is also a solution of the same equation at the chosen constraints, different combinations of shapes within the corresponding category are possible, provided that the combined shape fulfills the constraints [20]. In these cases, the Lagrange multipliers may be interdependent [19, 18, 10].

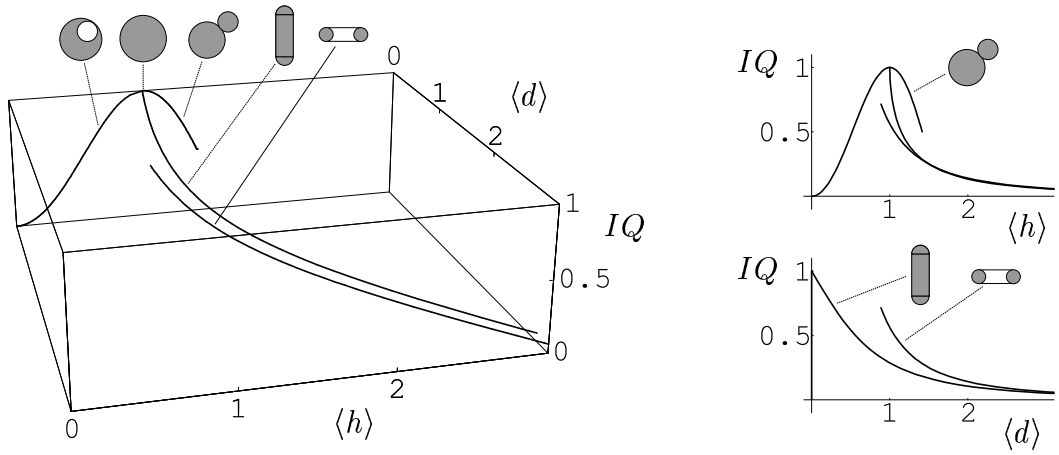

Figure 4. The ($\langle h\rangle$, $\langle d\rangle$, IQ) phase diagram. The lines pertaining to three sets of limiting shapes are depicted: the set of shapes composed of two spheres, the set of shapes composed of a cylinder ended by two hemispheres and the set of tori. The corresponding projections on the $\langle d\rangle = 0$ plane and on the $\langle h\rangle = 0$ plane are also shown (from [16]).

The equilibrium shapes can be characterized by the volume to area ratio defined as the isoperimetric quotient $IQ = 36\pi V^2/A^3$ and both average invariants of the curvature tensor. Dimensionless quantities are used to represent the average invariants: the dimensionless average mean curvature is $\langle h\rangle = R\langle H\rangle$ and the dimensionless average curvature deviator is $\langle d\rangle = R\langle D\rangle$, where $R = \sqrt{A/4\pi}$. The possible equilibrium shapes can be represented in a ($\langle h\rangle$, $\langle d\rangle$, IQ) phase diagram. The shapes of extreme average invariants of the curvature tensor form curves in this phase diagram (Fig. 4). These lines in turn form limits of the trajectories that correspond to the processes with changing average curvature invariants.

Fig. 5 shows the budding of a spherical vesicle from a planar lipid bilayer with increasing average mean curvature. All the shapes in the sequence but the first and the last are obtained by minimization of the membrane bending energy [22]. The first and the last shape are obtained by the solution of the

Figure 5. The sequence of shapes simulating the budding of a spherical vesicle from a planar lipid bilayer. The average mean curvature increases from left to right (from [22]).

variational problem of the extreme average mean curvature of a segment with fixed area ($\lambda_V = 0$). It can be seen that the limiting shape corresponding to the minimal average mean curvature consists of a section of a sphere while the limiting shape corresponding to the maximal average mean curvature consists of a segment of a flat surface and a spherical vesicle [21, 22, 23].

5. STATISTICAL MECHANICAL DESCRIPTION OF THE MEMBRANE

5.1. Statistical mechanical description of a bilayer membrane composed of only one kind of constituents

The contribution to the membrane free energy due to local interaction between the molecules and the mean curvature field is in the first approximation obtained by summing the contributions of the individual molecules of both layers [12],

$$F = \int m_{\mathrm{out}}\, F_{\mathrm{i}}(C_1,\, C_2)\, \mathrm{d}A + \int m_{\mathrm{in}}\, F_{\mathrm{i}}(-C_1,\, -C_2)\, \mathrm{d}A, \tag{26}$$

where m_{out} and m_{in} are the area densities of the molecules in the outer and the inner membrane layer, respectively, while F_{i} is given by Eq. (16). The integration is performed over the membrane area A. Note that the principal curvatures in the inner layer have signs opposite to the signs of the principal curvatures of the outer layer due to the specific configuration of the phospholipid molecules within the layers - touching by the tails.

If we assume for simplicity that the area densities are constant over the respective layers and also equal, $m_{\mathrm{out}} = m_{\mathrm{in}} = m_0$, and insert the expression for the single-molecule energy (Eq. (16)) into Eq. (26), we obtain [12]

$$\begin{aligned} F &= m_0\, \xi \int H^2\, \mathrm{d}A + m_0 \frac{\xi + \xi^\star}{2} \int D^2\, \mathrm{d}A - \\ &- 2 m_0\, k\, T \int \ln\Big(\mathrm{I}_0\big(\frac{\xi + \xi^\star}{2k\, T} D_{\mathrm{m}}\, D\big)\Big)\, \mathrm{d}A. \end{aligned} \tag{27}$$

In integrating, the differences in the areas of the inner and the outer layer were disregarded, so that the contributions proportional to the intrinsic mean curvature H_{m} of the inner and the outer layer cancel and there is no spontaneous curvature for bilayer vesicles composed of a single species of molecules. Also, the constant terms were omitted from Eq. (27).

The above procedure leading to Eq. (27) is a statistical mechanical derivation of the expression of continuum elastomechanics. It can be seen from Eq. (27) that the free energy of the membrane inclusions is expressed in a simple

and transparent way by the two invariants of the local curvature tensor: by the mean curvature and the curvature deviator.

The first and the second term of Eq. (27) can be combined by using Eq. (15) to yield [12]

$$F = m_0 \frac{3\xi + \xi^\star}{8} \int (2H)^2 \, \mathrm{d}A - m_0 \frac{\xi + \xi^\star}{2} \int C_1 \, C_2 \, \mathrm{d}A \\ -2k\,T\,m_0 \int \ln\Big(\mathrm{I}_0\big(\frac{\xi + \xi^\star}{2k\,T}\, D_\mathrm{m}\, D\big)\Big) \, \mathrm{d}A, \tag{28}$$

as to compare the expression (28) to the bending energy of an almost flat thin membrane [3] with zero spontaneous curvature

$$W_\mathrm{b} = \frac{k_c}{2} \int (2H)^2 \, \mathrm{d}A + k_\mathrm{G} \int C_1 \, C_2 \, \mathrm{d}A, \tag{29}$$

where k_c and k_G are the membrane local and Gaussian bending constants, respectively. We can see that the statistical mechanical derivation recovers the expression (29), where

$$m_0(3\xi + \xi^\star)/4 = k_\mathrm{c} \tag{30}$$

and

$$-m_0(\xi + \xi^\star)/2 = k_\mathrm{G}, \tag{31}$$

and yields also an additional contribution (third term in Eq. (28)) due to the orientational ordering of the phospholipid molecules. This contribution, which is always negative, is called the deviatoric elastic energy of the membrane (originating in the curvature deviator D (Eq. (14))). Also, it follows from Eqs. (28) and (29) that the saddle splay modulus is negative for a one-component bilayer membrane.

5.1.1. Estimation of the strength of the deviatoric effect in a phospholipid bilayer membrane

Introducing the dimensionless quantities, the free energy F (Eq. (28)) is normalized by $2\pi\, m_0(3\xi + \xi^\star)$,

$$f = \frac{1}{4} \int (2h)^2 \, \mathrm{d}a + \kappa_G \int c_1 \, c_2 \, \mathrm{d}a - \kappa \int \ln\big(\mathrm{I}_0(\vartheta \, d_\mathrm{m} \, d)\big) \, \mathrm{d}a, \tag{32}$$

where $\mathrm{d}a = \mathrm{d}A/4\pi\,R^2$, $R = (A/4\pi)^{1/2}$, $\kappa_G = -(\xi + \xi^\star)/(3\xi + \xi^\star)$, $\kappa = 4k\,T\,R^2/(3\xi + \xi^\star)$, $\vartheta = (\xi + \xi^\star)/2k\,T\,R^2$, $c_1 = R\,C_1$, $c_2 = R\,C_2$, $h = R\,H$, $d = R\,D$ and $d_\mathrm{m} = R\,D_\mathrm{m}$. We also obtain the dimensionless bending energy w_b if we normalize the expression (29) by $8\pi\,k_c$. Thereby, $\kappa_G = k_G/2k_c$.

To estimate the interaction constants, we assume that the conformation of the phospholipid molecules is equal all over the membrane and for simplicity take that $\xi = \xi^\star$. In this case, $\kappa_G = -1/2$, so that $k_G = -k_c$. By comparing the constants before the first terms of Eqs. (28) and (29) we can express the interaction constant ξ by measured quantities: the local bending constant k_c and the area density of the number of phospholipid molecules m_0, so that [12]

$$\xi = k_\mathrm{c}/m_0, \tag{33}$$

$$\kappa = 1/\vartheta = k\,T\,R^2\,m_0/k_\mathrm{c}. \tag{34}$$

We consider that $k_\mathrm{c} \simeq 20k\,T$ [24, 25] and that $m_0 = 1/a_0$ where a_0 is the area per molecule, $a_0 \simeq 0.6\,\mathrm{nm}^2$ [26], $T = 300\,\mathrm{K}$ and $R = 10^{-5}\,\mathrm{m}$. This gives $\kappa = 1/\vartheta \simeq 8.3 \cdot 10^6$. We estimate that the upper bound of D_m is the inverse of the molecular dimension ($\simeq 10^8\,\mathrm{m}^{-1}$) so that in our case $d_\mathrm{m} = R\,D_\mathrm{m}$ would be of the order of 10^3.

It follows from the above estimation that the argument of the Bessel function in Eq. (32) is very small unless $1/D$ is smaller than about a micrometre. In effect, the deviatoric contribution to the area density of the free energy of the phospholipid bilayer membrane is important only in those regions of the vesicle shape where there is a large absolute value of the difference between the two principal curvatures.

5.2. Statistical mechanical description of anisotropic inclusions within the approximation of a two-dimensional ideal gas

It is imagined that the membrane layer is divided into patches that are so small that the curvature is constant over the patch; however, they are large enough to contain a large number of inclusions that can be treated by statistical methods. It is taken that the inclusions protrude through both membrane layers. A chosen patch is a system with a well defined curvature field $\underline{C}$, given area A^p, number of inclusions M and temperature T and can therefore be subject to a local thermodynamic equilibrium. To describe the local thermodynamic equilibrium we chose canonical statistics [27] where we treat the inclusions as a two-dimensional ideal gas confined to the membrane surface. Within this approximation, the inclusions are treated as dimensionless and explicitly independent. The inclusions are also considered as indistinguishable. The canonical partition function of the inclusions in the small patch of the membrane is $Q = q^M/M!$, where q is the partition function of the inclusion (Eq. (9)) and M is the number of inclusions in the patch. Knowing the canonical partition function of the patch Q, we obtain the Helmholtz free energy of the patch, $F^\mathrm{p} = -k\,T\,\ln Q$. The Stirling approximation is used

and the area density of the number of molecules $m = M/A^{\mathrm{p}}$ is introduced. This gives for the area density of the free energy [15]

$$\frac{F^{\mathrm{p}}}{A^{\mathrm{p}}} = -k\,T\,m\,\ln\Big(q_{\mathrm{c}}\,\mathrm{I}_0\big(\frac{\xi+\xi^\star}{2k\,T}\,D_{\mathrm{m}}\,D\big)\Big) + k\,T(m\ln m - m). \tag{35}$$

To obtain the free energy of the whole membrane F_{m} the contributions of all the patches are summed, *i.e.*, integration over the membrane area A is performed

$$F_{\mathrm{m}} = \int \frac{F^{\mathrm{p}}}{A^{\mathrm{p}}}\,\mathrm{d}A. \tag{36}$$

The explicit dependence of the area density m on position can be determined by the condition for the free energy of all the membrane inclusions to be at its minimum in the thermodynamic equilibrium $\delta F_{\mathrm{m}} = 0$. It is taken into account that the total number of inclusions M_{T} in the membrane is fixed,

$$\int_A m\,\mathrm{d}A = M_{\mathrm{T}} \tag{37}$$

and that the area of the membrane A is fixed. The above isoperimetric problem is reduced to the ordinary variational problem by constructing a functional

$$F_{\mathrm{m}} + \lambda_m \int_A m\,\mathrm{d}A = \int_A \mathcal{L}(m)\,\mathrm{d}A, \tag{38}$$

where

$$\mathcal{L}(m) = -k\,T\,m\,\ln\Big(q_{\mathrm{c}}\,\mathrm{I}_0\big(\frac{\xi+\xi^\star}{2k\,T}\,D_{\mathrm{m}}\,D\big)\Big) + k\,T(m\,\ln m - m) + \lambda_m\,m \tag{39}$$

and λ_m is the Lagrange multiplier. The variation is performed by solving the Euler equation $\partial\mathcal{L}/\partial m = 0$. Deriving (39) with respect to m and taking into account Eq. (37) gives the Boltzmann distribution function modulated by the modified Bessel function I_0 [15]

$$\frac{m}{m_{\mathrm{u}}} = \frac{q_{\mathrm{c}}\,\mathrm{I}_0\big(\frac{\xi+\xi^\star}{2k\,T}\,D_{\mathrm{m}}\,D\big)}{\frac{1}{A}\int q_{\mathrm{c}}\,\mathrm{I}_0\big(\frac{\xi+\xi^\star}{2k\,T}\,D_{\mathrm{m}}\,D\big)\,\mathrm{d}A}, \tag{40}$$

where q_{c} is given by Eq. (10) and m_{u} is defined by $m_{\mathrm{u}}\,A = M_{\mathrm{T}}$.

To obtain the equilibrium free energy of the inclusions the expression for the equilibrium area density (Eq. (40)) is inserted into Eq. (35) and integrated over the area A. Rearranging the terms yields [15]

$$F_{\mathrm{m}} = -k\,T\,M_{\mathrm{T}}\ln\Big(\frac{1}{A}\int q_{\mathrm{c}}\,\mathrm{I}_0\big(\frac{\xi+\xi^\star}{2k\,T}\,D_{\mathrm{m}}\,D\big)\,\mathrm{d}A\Big). \tag{41}$$

The equilibrium free energy of the inclusions cannot in general be expressed as an integral of the area density of the free energy. We say that the contribution of the inclusions is a nonlocal one. A change of the local conditions affects the cell shape and the distribution of the inclusions through the minimization of the free energy of the whole membrane. Although the inclusions are explicitly treated as independent, their mutual influence is taken into account through the mean curvature field which in turn depends on the lateral and orientational distribution of the inclusions. It can also be seen from Eq. (41) that the energy of the membrane with inclusions is not scale invariant. The inclusions favour a certain packing arrangement that depends on the values of the principal membrane curvatures.

To estimate the strength of the deviatoric effect, the free energy F_{m} (Eq. (41)) is normalized by $8\pi\, k_{\mathrm{c}}$

$$f_{\mathrm{m}} = -\kappa_{\mathrm{m}} \ln \int \left(q_{\mathrm{c}}\, \mathrm{I}_0(\vartheta\, d_{\mathrm{m}}\, d)\right) \mathrm{d}a, , \tag{42}$$

where $\kappa_{\mathrm{m}} = M_{\mathrm{T}}\, k\, T/8\pi\, k_{\mathrm{c}}$, $\vartheta = (\xi + \xi^{\star})/2k\, T\, R^2$, while h, d, d_{m}, R and $\mathrm{d}a$ are defined as below Eq. (32). We took $\xi = \xi^{\star}$, $\kappa_{\mathrm{m}} = 1$, $H_{\mathrm{m}} = h_{\mathrm{m}}/R = 0$, $D_{\mathrm{m}} = 1/300\ \mathrm{\AA}^{-1}$ and $R = 6\mu\,\mathrm{m}$ [15]. The interaction constant ξ was estimated by assuming that the energy cost of distorting the tail of a phospholipid molecule within the inclusion is approximately equal to the energy difference corresponding to the tail packing in different aggregation geometries. Such a difference is of the order of (0.1 - 0.5) $k\,T$ per tail of a phospholipid molecule [28]. If we assume that there are 10 molecules (20 tails) involved in the inclusion, the energy of the inclusion can reach several $k\,T$. For the mother cell $h \simeq 1$ while $d \simeq 0$. Then, from the above choice of h_{m} and d_{m} and Eq. (6), we estimated that ϑ is of the order of 10^{-3}.

Fig. 6 shows the relative free energy of the inclusions f_{m} and the relative membrane bending energy w_{b} as a function of increasing average mean curvature $\langle h \rangle$ for a sequence in which the shape with one spherical vesicle is formed from a pear shape. The shapes in the sequence correspond to the minimum of the membrane bending energy. It can be seen that the bending energy monotonously increases along the sequence. The free energy of the inclusions only slightly decreases as long as the neck is wide. When the neck shrinks, the free energy of the inclusions sharply decreases, reaches a minimum and then increases towards the initial value. When the neck becomes infinitesimal, the curvature deviator becomes very large, however, the area of the neck becomes very small. The deep minimum of the $f_{\mathrm{m}}(\langle h \rangle)$ curve provides a possible explanation for the stability of thin necks connecting the daughter vesicle and the mother cell [29].

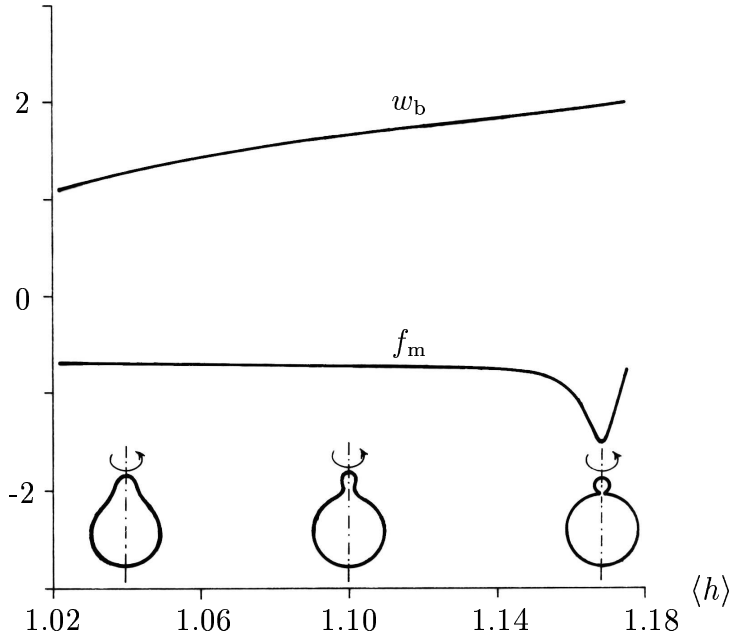

Figure 6. The normalized free energy of the inclusions f_m (Eq. (42)) and the normalized membrane bending energy w_b (first term of Eq. (32)) as a function of increasing normalized average mean curvature $\langle h \rangle$; $\vartheta = 10^{-3}$, $\kappa_m = 1$, $h_m = 0$, $d_m = 100$ and $IQ = 0.9$. The energy f_m is determined up to a constant (adapted from [15]).

6. MEMBRANE SHAPES EXHIBITING DEVIATORIC ELASTICITY

6.1. Myelin-like protrusions of phospholipid bilayer vesicles

An experiment showing fast recovery of fluorescence in photobleached giant phospholipid vesicles [30] indicated that the giant phospholipid vesicles obtained in the process of electroformation [31] are connected by thin tubular structures [30]. Later, it was observed [32] that giant palmitoyloleylphosphatidylcholine (POPC) bilayer vesicles, which immediately after formation appear spherical, spontaneously transform into flaccid fluctuating vesicles in a process where the remnants of thin tubular structures that are attached to the vesicles become thicker and shorter and eventually integrate into the membrane of the mother vesicle. The thin tubular network acts as a reservoir for the membrane area and importantly influences the future shape and dynamics of the globular phospholipid vesicles.

The POPC vesicles were prepared and observed in sugar solution [32] and in pure water [12]. Also, the vesicles were labelled with the fluorescent probe NBD-PC [32]. The observed features are the same in all cases. Immediately after being placed into the observation chamber the vesicles are spherical; the protrusions are not visible under phase contrast and the long

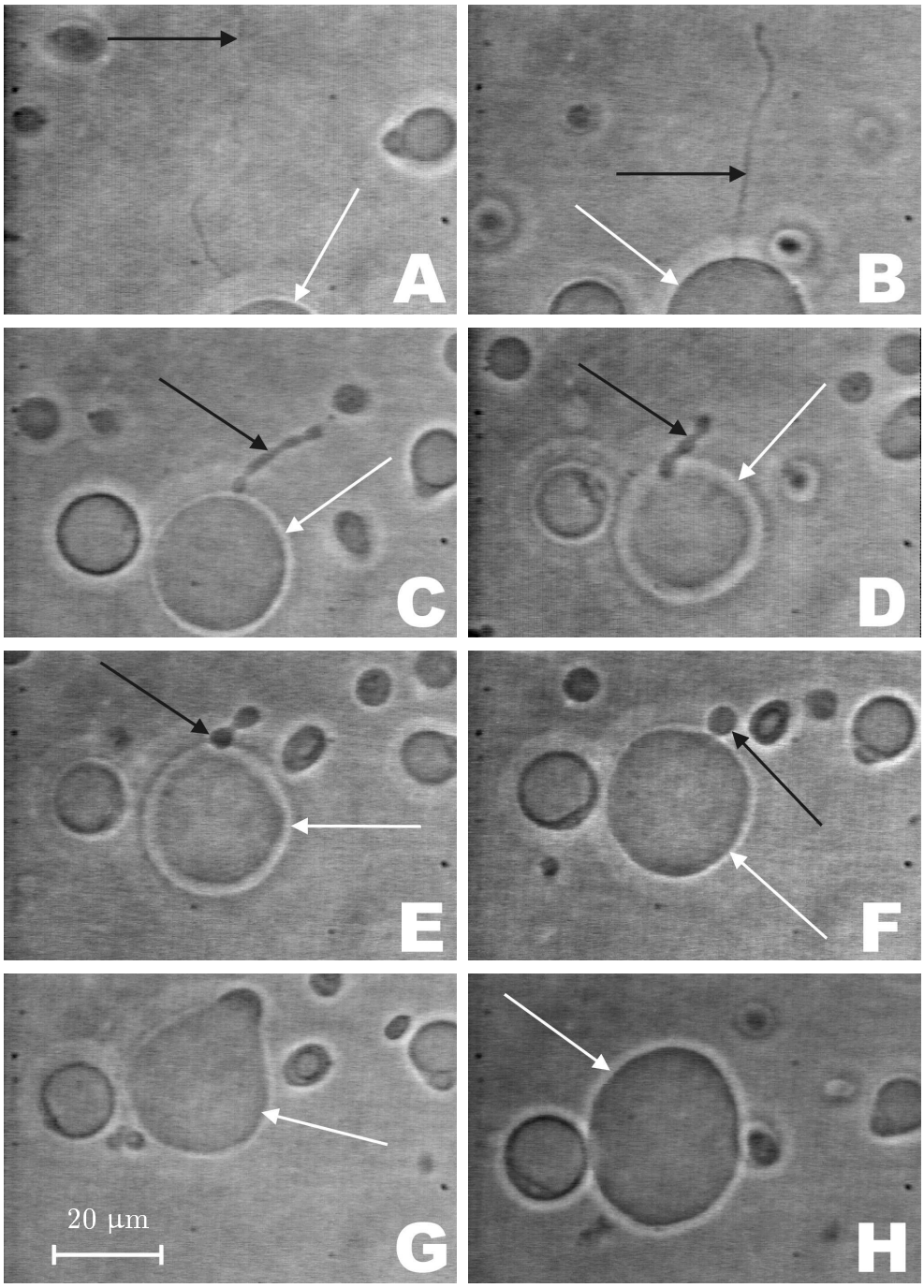

Figure 7. Shape transformation of a giant phospholipid vesicle (made of POPC and 1.5 % NBD-PC in sugar solution) with time. The times after the preparation of the vesicles are A: 3 h, B: 3 h 20 min, C: 4 h, D: 4 h 2 min, E: 4 h 4 min 30 s, F: 4 h 8 min 15 s, G: 4 h 14 min 25 s, H: 4 h 14 min 30 s. The white arrows indicate the protrusion while the black arrows indicate the mother vesicle. The vesicle was observed under an inverted Zeiss IM 35 microscope with phase contrast optics (from [32]).

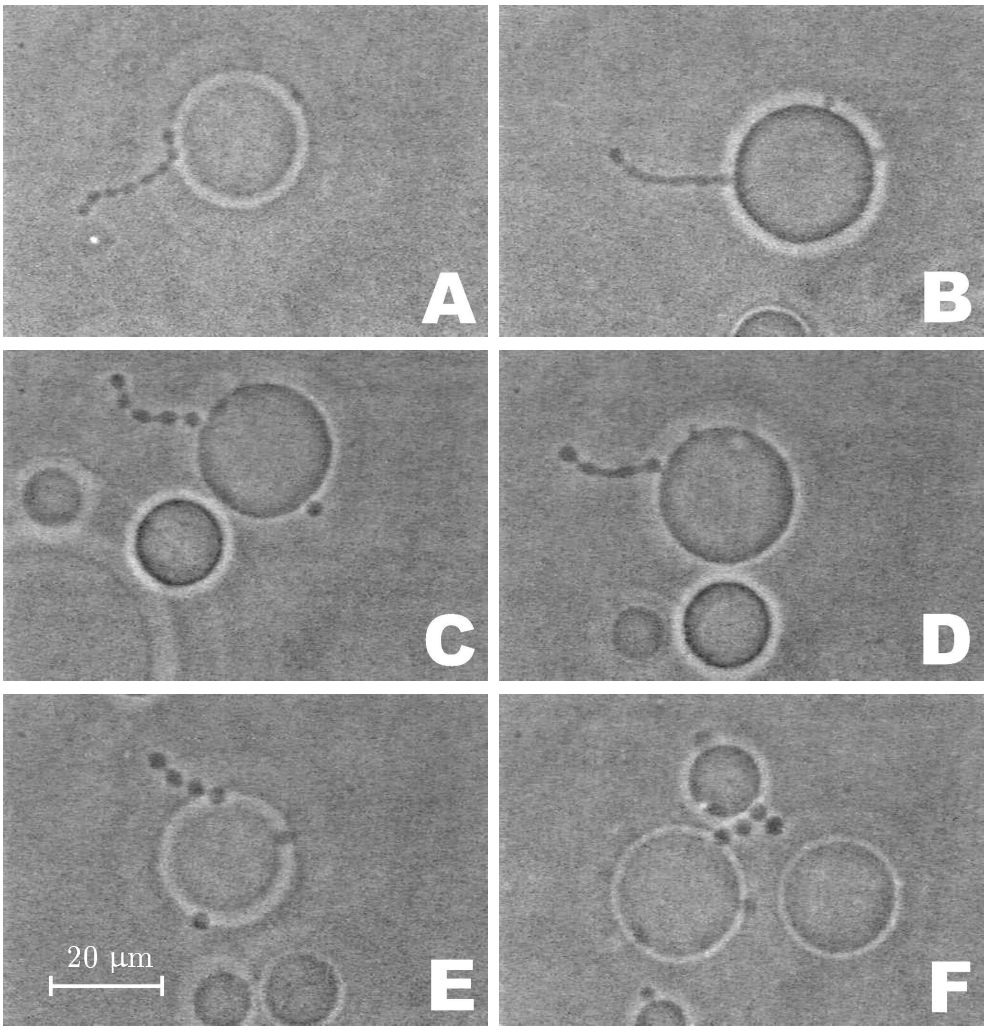

Figure 8. Shape transformation of a giant phospholipid vesicle (made of POPC in sugar solution as in [32]) with time. A small void was left in the grease closing the observation chamber to allow water evaporation. Undulations of the protrusion were observed at longer protrusions. When the "beads" became sphere-like (F), the shape stayed stable for about two hours. The vesicle was observed under an inverted Zeiss IM 35 microscope with phase contrast optics.

wavelength fluctuations of the spherical part are not observed. After some time, long thin protrusions become visible (Fig. 1C); the protrusions appear as very long thin tubes that are connected to the mother vesicle at one end while the other end is free. With time, the protrusion becomes shorter and thicker; however the tubular character of the protrusion is still preserved (Fig. 7A-C) while the fluctuations of the mother vesicle increase in strength. Later, undulations of the protrusion appear and become increasingly apparent. Shortened protrusions look like beads connected by thin necks (Fig. 7D-F). Eventually, the protrusion is completely integrated into the vesicle membrane to yield a fluctuating globular vesicle (Fig. 7H). The transformation of the protrusion is usually very slow, indicating that all the observed shapes may be considered as quasiequilibrium shapes. In the sample, the tubular protrusions are still observed several hours after the formation of the vesicles. The timing of the transformation may vary from minutes to hours, as the protrusions are initially of very different lengths.

The observed shape transformation may be driven by the inequality of the chemical potential of the phospholipid molecules in the outer solution and in the outer membrane layer which causes a decrease of the difference between the outer and the inner membrane layer areas. Possible mechanisms that were suggested to contribute to this are the drag of the lipid from the outer solution by the glass walls of the chamber, chemical modification of the phospholipid and phospholipid flip-flop [32]. A decrease of the volume to area ratio (isoperimetric quotient) of the vesicle occurs due to slight evaporation of water from the chamber. The vesicle then looses water in order to equalize the respective chemical potentials inside and outside the vesicle. The tubular/beadlike character of the protrusion seems to depend on the speed of the loss of lipid molecules from the outer membrane layer relative to the speed of the decrease of the enclosed volume. The undulations of the protrusion are more evident when a small void is left in the grease thereby enhancing the evaporation of water from the outer solution (Fig. 8).

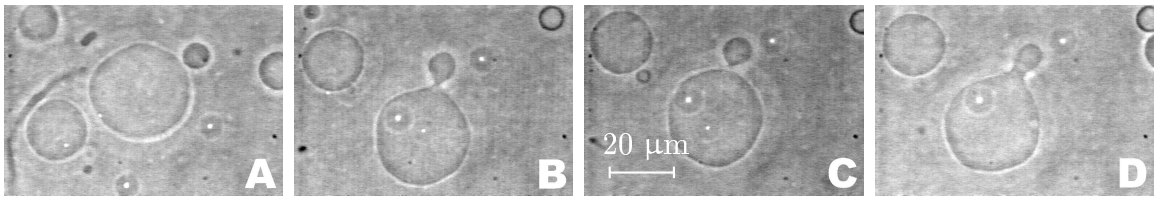

Figure 9. Oscillations of the neck width before opening of the neck of giant phospholipid (POPC) vesicle.

Another interesting observed feature is oscillation of the neck width. This is especially notable before the opening of the neck that connects the last bead with the mother vesicle (Fig. 7F-H). The neck shrinks and widens several times before the last bead integrates with the mother vesicle (Fig. 9) indicating increased stability of the neck. A similar effect - the persistence of the neck connecting a spherical daughter vesicle and a mother vesicle - was also observed in the opening of the neck induced by cooling, while the formation of the neck by heating was quick and took place at higher temperature, indicating hysteresis [33]. In the case when a small void is left in the observation chamber longer protrusions already have a beadlike form (Fig. 8). When the protrusion undergoes transformation into a shape with one bead less, the necks open to yield an almost tubular shape (Fig. 8B,D). If the protrusion develops into spherical beads connected by very thin necks (Fig. 8F), the shape stays stable for hours.

A complete picture of the dynamics of shape transformation seems at this point beyond our understanding. However, we can point to some facts that can be elicited with a certain confidence. In comparing the protrusions at an early time and at a later time, the protrusions at the early time appear considerably more tubular. Therefore we think that the protrusions also have tubular character even at earlier times when they are too thin to be seen by the phase contrast microscope. The possibility should be considered that the radius of the tubular protrusion immediately after its formation is very small - as small as the membrane thickness.

To describe these features theoretically, the equilibrium shape is determined by the minimum of the membrane free energy (Eq. (28)) under given constraints. It is considered that the membrane area A, the enclosed volume V and the average mean curvature are fixed. The average mean curvature of a thin membrane is proportional to the difference between the two membrane layer areas, $\langle H \rangle = \Delta A / 2A\,\delta$, where δ is the distance between the two layer neutral areas which is considered to be small with respect to $1/H$ and $\Delta A = \delta \int (C_1 + C_2) \mathrm{d}A$. The constraint for $\langle H \rangle$ therefore reflects the number of molecules that compose the respective layers and therefore the conditions in which the vesicle formation took place. If the area difference is normalized by $8\pi\delta R$ ($\Delta a = \Delta A / 8\pi\delta R$), for a thin bilayer, it is equal to the normalized average mean curvature,

$$\langle h \rangle = \Delta a = \frac{1}{2} \int (c_1 + c_2) \mathrm{d}a. \tag{43}$$

For the sake of simplicity, we compare two shapes that represent the limits of the class of shapes with a long thin protrusion. In the first case the protrusion consists of equal small spheres (Fig. 10A), while in the second

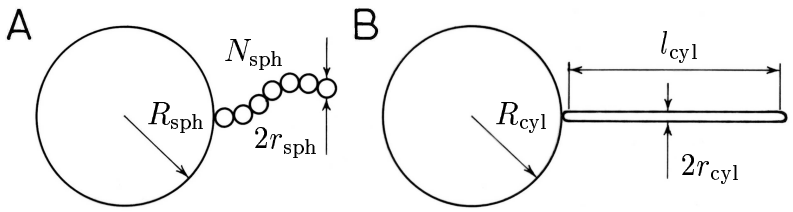

Figure 10. A: schematic presentation of a shape composed of the mother sphere and protrusion composed of small spheres connected by infinitesimal necks, B: schematic presentation of a shape composed of the mother sphere and a thin cylinder closed by hemispherical caps (from [12]).

case the protrusion consists of a cylinder closed by hemispherical caps (Fig. 10B). It is expected that these two shapes are continuously connected by a sequence of shapes with decreasingly exhibited undulations of the protrusion.

Each of these two limiting cases involves three geometrical model parameters (Fig. 3) that can be determined from geometrical constraints for the area, volume and average mean curvature. In the limit $IQ \simeq 1$, the geometrical parameters and therefore also the energies can be expressed analytically [12]. It has been shown that the relative membrane bending energy of the shape with the cylindrical protrusion $w_{\mathrm{b,\,cyl}}$ is always higher than the membrane bending energy of the shape with the spherical beads $w_{\mathrm{b,\,sph}}$ [12],

$$w_{\mathrm{b,\,cyl}} = w_{\mathrm{b,\,sph}} + 1. \tag{44}$$

As within the theory of elasticity of an isotropic bilayer membrane [3] the shape with a protrusion composed of small spheres that are connected by infinitesimal necks would always be favoured over the shape with a tubular protrusion (Eq. (44)), this theory is unable to explain stable tubular protrusions.

A possible mechanism that can explain the stability of the long thin tubular protrusions is that of a deviatoric elasticity which is a consequence of the orientational ordering of the membrane constituent molecules in the thin tubular protrusion. If we chose high $\langle h \rangle$ the shape has a long protrusion. As the membrane area and the enclosed volume are fixed, this protrusion is very thin and consequently its mean curvature is large. For tubular protrusions the deviatoric contribution to the normalized free energy (f_{d}) (third term in Eq. (32))

$$f_{\mathrm{d}} = -\kappa \int \ln\bigl(\mathrm{I}_0(\vartheta\, d_{\mathrm{m}}\, d)\bigr)\, \mathrm{d}a \tag{45}$$

is large enough to compensate for the less favourable bending energy of the cylinder Eq. (44). On the other hand, for lower $\langle h \rangle$, a protrusion of the same

membrane area and enclosed volume is shorter and broader, and therefore its mean curvature is lower. The corresponding deviatoric term of the cylinder is therefore too small to be of importance and the shape with the beadlike protrusion has lower free energy. At a chosen intrinsic anisotropy d_{m}, the shapes with small spheres are energetically more favourable below a certain $\langle h \rangle$ while above this threshold the shapes with cylinders are favoured.

Fig. 11 shows a $(\langle h \rangle, d_{\mathrm{m}})$ phase diagram exhibiting the regions corresponding to the calculated stable shapes composed of a spherical mother vesicle and a tubular protrusion and to a stable shapes composed of a spherical mother vesicle and a protrusion consisting of small spheres connected by infinitesimal necks.

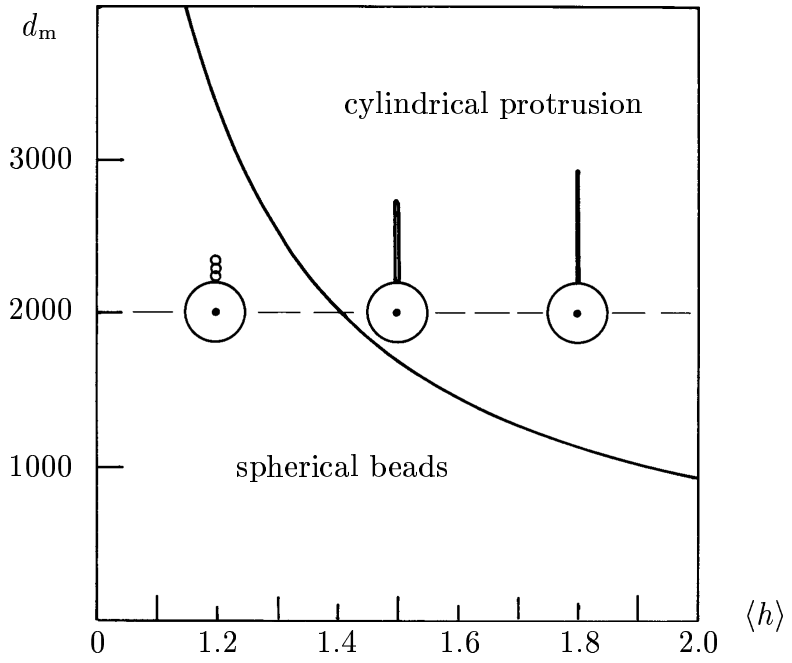

Figure 11. The $(\langle h \rangle, d_{\mathrm{m}})$ phase diagram of calculated equilibrium shapes with protrusions. The regions where shapes with a particular kind of protrusion are energetically more favourable are indicated. The sequence of shapes shown in the figure indicates the process of diminishing $\langle h \rangle$ at constant IQ that could be observed experimentally. We chose $a_0 = 0.6\ \mathrm{nm}^2$, $R = 10^{-5}$ m, $k_{\mathrm{c}} = 20\,kT$, so that $\kappa = 1/\vartheta = 8.3 \cdot 10^6$ while $IQ = 0.90$. The shapes corresponding to different $\langle h \rangle$ are depicted with the centre of the spherical part at the corresponding $\langle h \rangle$ values (adapted from [12]).

The radii of the stable tubular protrusion are $200 - 400$ nm while the corresponding deviatoric energies are larger than the estimated energy of thermal fluctuations [12]. The sequence of shapes shown in the figure roughly simulates the transformation observed experimentally (Fig. 7). Initially,

$\langle h \rangle$ is large and the shape is composed of a mother sphere and a long thin nanotube. Assuming that the volume of the vesicle remains constant with time, the number of phospholipid molecules in the outer layer diminishes, so that $\langle h \rangle$ decreases and the tubular protrusion becomes thicker and shorter. In the experiment [32], the undulations of the protrusion became increasingly notable during the process. Our theoretical results shown in Fig. 11 exhibit a discontinuous transition from a tubular protrusion to a protrusion composed of small spheres connected by infinitesimal necks, as we consider only the limits of the given class of shapes. Therefore, the phase diagram and the sequence (Fig. 11) should be viewed only as an indication of the trend of shape transition and not as to the details of the shape.

6.2. Detergent-induced anisotropic structures of the erythrocyte membrane

Continuous intercalation of detergent molecules into the outer layer of the erythrocyte membrane eventually leads to microexovesiculation [7, 8, 9]. Upon intercalation of the detergent molecules into the membrane the mother-cell becomes spherical while a few percent of the erythrocyte membrane area is released in the form of microexovesicles. Analysis of the protein composition of the isolated microexovesicles [9, 21] showed that the microexovesicles are depleted in the membrane skeletal components spectrin and actin, suggesting that a local disruption of the interactions between the membrane skeleton and the membrane bilayer occurrs prior to microexovesiculation [7, 9, 34, 21] and indicating that the shape of the microexovesicles is determined by the properties of the membrane.

It was observed [8] that some species of added amphiphiles induce predominantly spherical microexovesicles while other species induce predominantly tubular microexovesicles. Among these, the cationic dimeric amphiphile dioctyldiQAS, in which two head - tail entities are connected by a spacer at the headgroup level, induces stable tubular microexovesicles [10] (Fig. 13). An elongated tubular shape was exhibited even in the buds (Fig. 1B). For comparison, Fig. 1A shows budding of a spherical vesicle.

Fig. 13 shows a sequence of prolate shapes connecting two limiting shapes: the shape composed of a cylinder and two hemispherical caps and the shape composed of three spheres connected by infinitesimal necks. The corresponding normalized average mean curvatures and normalized average curvature deviators are also depicted. It can be seen that the shape composed of spheres corresponds to the maximal average mean curvature and minimal average curvature deviator while the shape composed of the cylinder and two hemispherical caps corresponds to the maximal average curvature deviator and minimal average mean curvature.

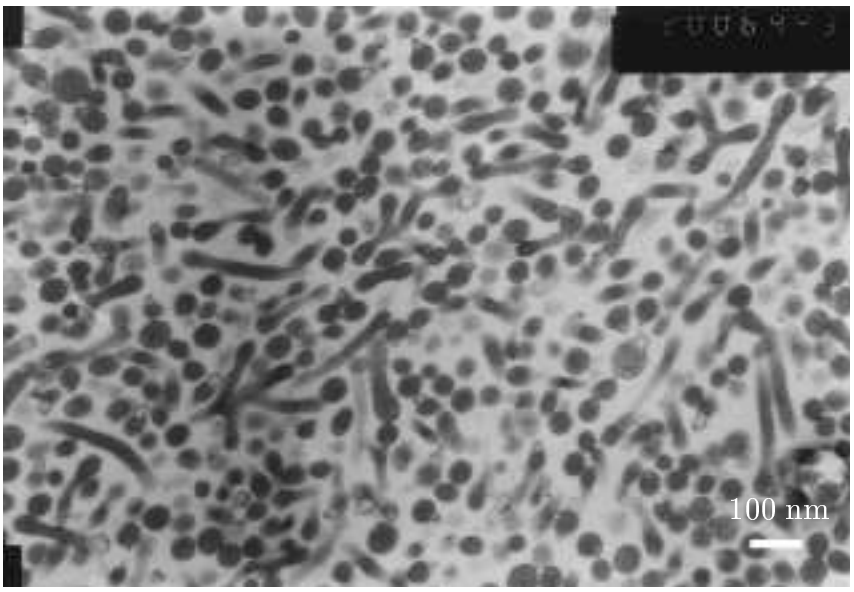

Figure 12. TEM image of the isolated tubular daughter microexovesicles induced by adding dioctyldiQAS to an erythrocyte suspension (from [10]).

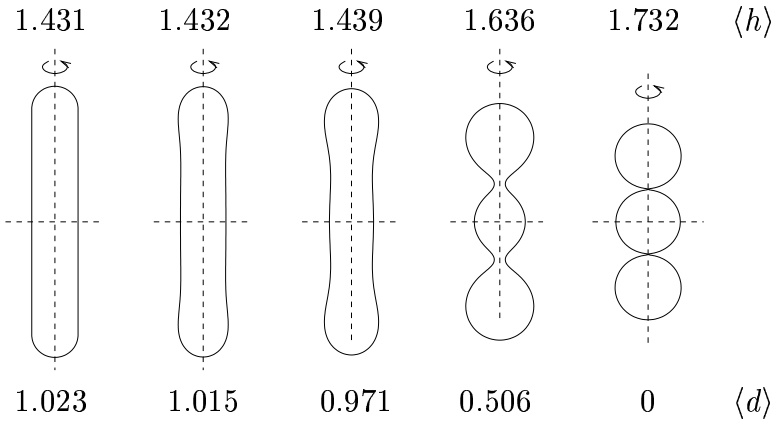

Figure 13. A sequence of axisymmetric vesicle shapes with $IQ = 1/3$. The corresponding values of the average mean curvature $\langle h \rangle$ and of the average curvature deviator $\langle d \rangle$ are given. All the shapes but the first from the left were obtained by minimizing the membrane bending energy. The first shape from the left was obtained by combining the solutions of Eq. (25) representing the sphere and the cylinder (adapted from [10]).

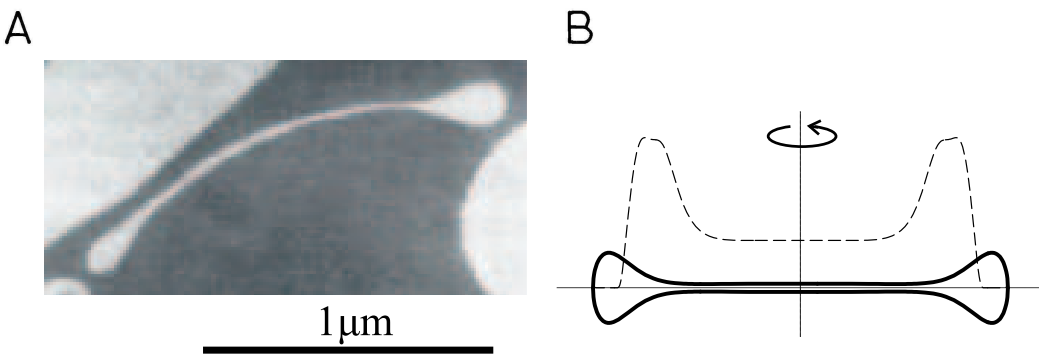

Figure 14. A: TEM micrograph of the torocyte endovesicle induced by adding $C_{12}E_8$ to an erythrocyte suspension (from [11]), B: calculated equilibrium shape of the torocyte (full line) and the corresponding distribution of the anisotropic inclusions (broken line); $\kappa_m = 100$, $\vartheta = 1$, $h_m = -1.5$, $d_m = 1.5$ (adapted from [16, 40]).

After adding both, dodecylzwittergent or dioctyldiQAS, to the erythrocyte suspension, the erythrocytes first underwent a discocyte-echinocyte-spheroechynocyte transformation [10, 35], so it is evident that the average mean curvature $\langle h \rangle$ continuously increased in the process [35]. According to the bilayer couple model [5, 36, 37, 38, 39, 35] expressed by the bending of the laterally isotropic membrane [3], the process of increasing the area difference $\triangle A$ *i.e.* - $\langle h \rangle$ due to the intercalation of detergent molecules into the outer membrane layer would lead to the shape of the maximal average mean curvature *i.e.* to spherical microexovesicles (Fig. 13). While the bilayer couple model explains the spherical shape of the microexovesicles that are induced by intercalating dodecylzwittergent into the erythrocyte membrane, it cannot explain the tubular shape of the microexovesicles induced by dioctyldiQAS.

A possible mechanism that can explain the observed stable tubular microexovesicle shape is that of a deviatoric elasticity which is a consequence of the orientational ordering of the detergent-induced inclusions on the tubular buds/vesicles [17, 14, 15, 10]. Besides increasing the average mean curvature, the intercalation of anisotropic dioctyldiQAS-induced inclusions also increase the average curvature deviator [10]. If the second effect prevails, the process may continue until the limiting shape composed of cylinder and two hemispherical caps (Fig. 12), that corresponds to the maximal average curvature deviator, is reached.

On the other hand, continuous intercalation of detergent molecules into the inner layer of the erythrocyte membrane eventually leads to endovesiculation. It was reported [11] that octaethyleneglycol dodecylether ($C_{12}E_8$)

may induce (usually one) stable endovesicle having a torocyte shape (Fig. 14A). It was observed that the torocyte endovesicle originates from a primarily large stomatocytic invagination which upon continuous intercalation of $C_{12}E_8$ molecules loses volume. The invagination may finally close, forming an inside-out endovesicle of small isoperimetric quotient. Three partly complementary mechanisms were suggested in order to explain the formation and stability of the observed torocytes [11, 18, 40]. The first is preferential intercalation of the $C_{12}E_8$ molecules into the inner membrane layer, the second is preference of the $C_{12}E_8$ induced inclusions for zero or slightly negative local mean curvature, and the third is the lateral and orientational ordering of $C_{12}E_8$ induced inclusions. It was suggested [40] that lipid molecules and membrane proteins may be involved in $C_{12}E_8$ induced inclusions. To determine the equilibrium shape of the torocyte endovesicle, the membrane free energy (including the free energy of the inclusions) is minimized at fixed membrane area and fixed enclosed volume [40]. Eq. (42) is used to calculate the free energy of the inclusions. Fig. 14 shows the calculated equilibrium shape of the torocyte vesicle and the corresponding distribution of the $C_{12}E_8$ induced inclusions. It can be seen that the inclusions favour the region of highly different main curvatures while the contour of the calculated shape agrees with the observed TEM image. In order to calculate the characteristic torocyte shape (Fig. 14B) it was necessary to include the deviatoric effect [16, 40]. Within the standard bending elasticity model of the bilayer membrane [3, 36, 37, 38, 39] the calculated torocyte vesicle shapes, corresponding to the minimal bending energy, have a thin central region where the membranes on the both sides of the vesicle are in close contact, *i.e.* the resultant forces on both membranes in contact are balanced [18]. However, as it can be seen in Fig. 14A the adjacent membranes in the flat central region are separated by a certain distance indicating that the stability of the observed torocyte shape can not be explained by the standard bending elasticity model.

The same substance, *i.e.* the detergent $C_{12}E_8$, was shown to stabilize transient pores in cell membrane that are created by electroporation [41]. By using a simple geometrical model of the pore where the pore was described as the inner part of the torus, and by minimizing the free energy of the inclusions (Eq. (42)), the equilibrium configuration of the system was predicted at a finite size of the pore - if the inclusions were anisotropic [42, 16].

The examples presented indicate that the model in which the membrane is treated as a laterally isotropic two dimensional liquid should be upgraded in order to describe the observed features. The deviatoric elasticity provides an explanation for some of the observed features; however, further refinement of the model such as inclusion of the role of the membrane skeleton [43, 44,

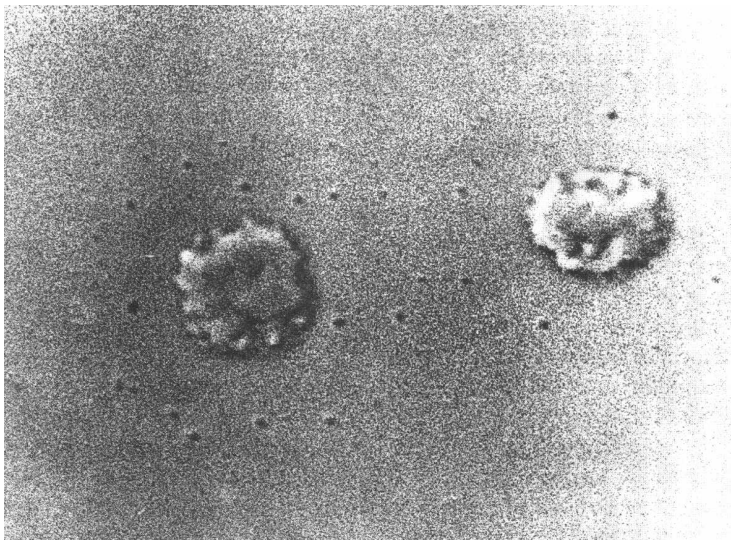

Figure 15. Vesiculation of human erythrocytes at high pH with exogeneously added dibucaine. The vesicles around the mother cell move synchronously with the mother cell indicating that they are connected to the mother cell by thin tethers (from [29]).

45, 46, 35, 47, 48] should be taken into account in order to obtain a more realistic description.

7. CONCLUSION

Considerable knowledge has been gathered on lipid bilayer membranes. The interdependence between the membrane elastic properties, the conditions in solution and the vesicle and cell shape has been thoroughly investigated [49, 3, 39, 50, 43, 51, 35, 52, 53]. Theoretical approaches based on statistical mechanical methods mostly describe the configuration of the hydrocarbon tails [54, 28, 55], while the link between the detailed description of the tails and the membrane shape has not been made. On the other hand, this link was achieved in describing the effect of membrane inclusions [56] on the vesicle shape [57, 14, 17, 15, 40]. Most of the work was devoted to globular shaped vesicles and cells where the membrane could be considered as an almost flat and laterally isotropic two-dimensional liquid [2].

Recently, the experiments have drawn attention to thin anisotropic structures attached to the globular part of the vesicle [30, 10, 32, 12]. Further, such structures seem to be common also in cells [29] (Fig. 15). It was indicated that these structures form an important auxiliary pool of the membraneous material that hitherto remained obscure. We have found that the features involving the auxiliary pool cannot be explained if the membrane is treated

as a two dimensional liquid. We propose a simple mechanism which considers that the membrane constituents are intrinsically anisotropic. While the collective effect on almost flat regions yields the state of a laterally isotropic two dimensional liquid, the anisotropic properties become expressed if the membrane for some reason develops regions of highly different main curvatures. The proposed mechanism provides an explanation for the stability of the phospholipid micro and nanotubes attached to the giant phospholipid vesicle, for the stability of thin tethers connecting the mother cell and the daughter vesicle in erythrocytes, for the stability of tubular daughter microexovesicles and torocytic daughter endovesicles of the erythrocyte membrane and for the stability of detergent-induced pores in the cell membrane. However, the auxiliary pool is yet to be explored.

REFERENCES

[1] H. Ti Tien and A.L. Ottova, J. Membr. Sci., 189 (2001) 83.
[2] S.J. Singer and G.L. Nicholson, Science, 175 (1972) 720.
[3] W. Helfrich, Z. Naturforsch., 28c (1973) 693.
[4] B. Deuticke, Biochim. Biophys. Acta, 163 (1968) 494.
[5] M.P. Sheetz and S.J. Singer, Proc. Natl. Acad. Sci. USA, 72 (1974) 4457.
[6] S. Schreier, S.V.P. Malherios and E. de Paula, Biochim. Biophys. Acta, 1508 (2000) 210.
[7] S.C. Liu, L.H. Derick, M.A. Duquette and J. Palek, Eur.J.Cell Biol., 49 (1989) 358.
[8] H. Hagerstrand and B. Isomaa, Biochim. Biophys. Acta, 1109 (1992) 117.
[9] H. Hagerstrand and B. Isomaa, Biochim. Biophys. Acta, 1190 (1994) 409.
[10] V. Kralj-Iglic, A. Iglic, H. Hagerstrand and P. Peterlin, Phys. Rev. E, 61 (2000) 4230.
[11] M. Bobrowska-Hagerstrand, V. Kralj-Iglic, A. Iglic, K. Bialkowska, B. Isomaa and H. Hagerstrand, Biophys. J., 77 (1999) 3356.
[12] V. Kralj-Iglic, A. Iglic, G. Gomiscek, F. Sevsek, V. Arrigler and H. Hagerstrand, J. Phys. A.: Math. Gen., 35 (2002) 1533.
[13] V. Kralj-Iglic, M. Remskar, M. Fosnaric, G. Vidmar and A. Iglic, Phys. Lett. A, 296 (2002) 151.
[14] V. Kralj-Iglic, S. Svetina and B. Zeks, Eur. Biophys. J., 24 (1996) 311.
[15] V. Kralj-Iglic, V. Heinrich, S. Svetina and B. Zeks, Eur. Phys. J. B, 10 (1999) 5.
[16] M. Fosnaric, A. Iglic and V. Kralj-Iglic, in: I.M. Mladenov and G.L. Naber (eds.), Geometry, Integrability and Quantization, Coral Press,

Sofia 2002, p.224.
[17] J.B. Fournier, Phys. Rev. Lett., 76 (1996) 4436.
[18] A. Iglic, V. Kralj-Iglic, B. Bozic, M. Bobrowska-Hagerstrand, B. Isomaa and H. Hagerstrand, Bioelectrochemistry, 52 (2000) 203.
[19] A. Iglic, V. Kralj-Iglic and J. Majhenc, J. Biomech., 32 (1999) 1343.
[20] L.E. Elsgolc, Calculus of Variations, Pergamon Press, Oxford, 1961.
[21] H. Hagerstrand, V. Kralj-Iglic, M. Bobrowska-Hagerstrand and A. Iglic, Bull. Math. Biol., 61 (1999) 1019.
[22] A. Iglic and H. Hagerstrand, Med. Biol. Eng. Comp., 37 (1999) 125.
[23] H. Hagerstrand, M. Danieluk, M. Bobrowska-Hagerstrand, V. Pector, J. M. Ruysschaert, V. Kralj-Iglic and A. Iglic, Biochim. Biophys. Acta, 1421 (1999) 125.
[24] H.P. Duwe, J. Kas and E. Sackmann, J. Phys. (France), 51 (1990) 945.
[25] U. Seifert, Adv. Phys., 46 (1997) 13.
[26] G. Cevc and D. Marsh, Phospholipid Bilayers, Wiley - Interscience, New York, 1987.
[27] T.R. Hill, An Introduction to Statistical Thermodynamics, Dover Publications, New York, 1986.
[28] A. Ben-Shaul and W.M. Gelbart, in: W.M.Gelbart, A. Ben-Shaul and D. Roux (eds.), Micelles, Membranes and Monolayers, Springer Verlag, New York, 1994, 47.
[29] V. Kralj-Iglic, A. Iglic, M. Bobrowska-Hagerstrand and H. Hagerstrand, Coll. Surf. A, 179 (2001) 57.
[30] L. Mathivet, S. Cribier and P.F. Devaux, Biophys. J., 70 (1996) 1112.
[31] M.I. Angelova, S. Soleau, Ph. Meleard, J.F. Faucon and P. Bothorel, Prog. Colloid Polym. Sci., 89 (1992) 127.
[32] V. Kralj-Iglic, G. Gomiscek, J. Majhenc, V. Arrigler and S. Svetina, Coll. Surf. A, 181 (2001) 315.
[33] J. Kas and E. Sackmann, Biophys.J., 60 (1991) 825.
[34] A. Iglic, S. Svetina and B. Zeks, Biophys. J., 69 (1995) 274.
[35] A. Iglic, V. Kralj-Iglic and H. Hagerstrand, Eur. Biophys. J., 27 (1998) 335.
[36] E.A. Evans, Biophys. J., 14 (1974) 923.
[37] W. Helfrich, Z. Naturforsch., 29c (1974) 510.
[38] E.A. Evans, Biophys. J., 30 (1980) 265.
[39] S. Svetina, A. Ottova-Leitmannova and R. Glaser, J. Theor. Biol., 94 (1982) 13.
[40] M. Fosnaric, M. Nemec, V. Kralj-Iglic, H. Hagerstrand, M. Schara and A. Iglic, Coll. Surf. B, 26 (2002) 243.
[41] G. Troiano, K. Stebe, V. Sharma and L. Tung, Biophys. J., 74 (1998) 880.

[42] M. Fosnaric, H. Hagerstrand, V. Kralj-Iglic and A. Iglic, Cell. Mol. Biol. Lett., 6 (2001) 167.
[43] A. Elgsaeter and A. Mikkelsen, Biochim. Biophys. Acta, 1071 (1991) 273.
[44] A. Iglic, J. Biomech., 30 (1997) 35.
[45] M. Bobrowska - Hagerstrand, H. Hagerstrand and A. Iglic, Biochim. Biophys. Acta, 1371 (1998) 123.
[46] R.E. Waugh, Biophys. J., 70 (1996) 1027.
[47] H. Hagerstrand, M. Danieluk, M. Bobrowska-Hagerstrand, A. Iglic, A. Wrobel, B. Isomaa and M. Nikinmaa, Biochim. Biophys. Acta, 1466 (2000) 125.
[48] H. Hagerstrand, M. Danieluk, M. Bobrowska-Hagerstrand, T. Holmstrom, V. Kralj-Iglic, C. Lindqvist and M. Nikinmaa, Mol. Membr. Biol., 16 (1999) 195.
[49] P.B. Canham, J. Theor. Biol., 26 (1970) 61.
[50] R. Lipowsky, Nature, 349 (1991) 475.
[51] L. Miao, U. Seifert, M. Wortis and H.G. Dobereiner, Phys. Rev. E, 49 (1994) 5389.
[52] M. Bobrowska-Hagerstrand, H. Hagerstrand, and A. Iglic, Biochim. Biophys. Acta, 1371 (1998) 123.
[53] A. Iglic, P. Veranic, U. Batista and V. Kralj-Iglic, J. Biomech., 34 (2001) 765.
[54] S. Marcelja, Biochim. Biophys. Acta, 367 (1974) 165.
[55] I. Szleifer, D. Kramer, A. Ben-Shaul, W.M. Gelbart and S.A. Safran, J. Chem. Phys., 92 (1990) 6800.
[56] S. Marcelja, Biochim. Biophys. Acta, 455 (1976) 1.
[57] S. Leibler and D. Andelman, J. Phys., 48 (1987) 2013.